Quantum Virial Coefficients via Path Integral Monte Carlo with Semi-classical Beads

Ramachandran Subramanian, Andrew J. Schultz and David A. Kofke

Abstract Conventionally, Path Integral Monte Carlo (PIMC) calculations are performed with 'classical beads' (beads interacting via a classical potential) by using the primitive approximation for the thermal density matrix. Higher order propagators of the thermal density matrix have been proven to achieve faster convergence and better precision in quantum calculations than using just the primitive approximation. Use of different propagators in PIMC leads to methods equivalent to performing PIMC with 'semi-classical beads' (beads interacting via a semi-classical potential). We examine the Takahashi-Imada (TI) propagator as well as an ad hoc semi-classical potential in PIMC calculations for computing the quantum second virial coefficient for helium-4. We compare the performance of the two approaches based on semi-classical beads against values computed from PIMC using conventional classical beads. We find that while the TI propagator has the same or marginally better precision compared to the classical case, it has the best convergence rate (with respect to number of path-integral beads) among the three approaches. The convergence rate of the ad hoc potential is marginally better than its classical counterpart, and its precision is approximately the same as the classical case.

Keywords Path integral Monte Carlo · Takahashi-Imada propagator · Quantum virial coefficients · Helium-4 · Thermal density matrix

1 Introduction

The thermal density matrix ρ plays a key role in Feynman's imaginary-time Path Integrals (PI) formalism and its application in Monte Carlo (MC) algorithms to compute physical properties of interest. In position space, it is given by [1–3]:

R. Subramanian · A.J. Schultz · D.A. Kofke (✉)
Department of Chemical and Biological Engineering, University at Buffalo,
The State University of New York, Buffalo, NY 14260-4200, USA
e-mail: kofke@buffalo.edu

R.Q. Snurr et al. (eds.), *Foundations of Molecular Modeling and Simulation*,
Molecular Modeling and Simulation, DOI 10.1007/978-981-10-1128-3_6

$$\rho(R, R'; \beta) = \left\langle R | e^{-\beta \mathcal{H}} | R' \right\rangle \tag{1}$$

where $R = \{\boldsymbol{r}_1, \boldsymbol{r}_2, \ldots \boldsymbol{r}_n\}$ and $\beta = 1/k_{\mathrm{B}}T$, with k_{B} Boltzmann's constant and T the temperature. A key property of the density matrix is that the product of two density matrices is also a density matrix:

$$\rho(R, R'; \beta_1) \times \rho(R, R'; \beta_2) = \rho(R, R'; \beta_1 + \beta_2) \tag{2}$$

This is because any operator (specifically the Hamiltonian operator $\mathcal{H}$ here) is commutative with any scalar multiple of itself. This exact property allows us to write down the following $(P-1)$-fold convolution:

$$\rho(R_0, R_P; \beta) = \int \cdots \int \mathrm{d}R_1 \, \mathrm{d}R_2 \ldots \mathrm{d}R_{P-1} \, \rho(R_0, R_1; \tau) \rho(R_1, R_2; \tau) \ldots \rho(R_{P-1}, R_P; \tau) \tag{3}$$

where $\tau = \beta/P$. Note that even though the above expression is exact, one needs to make approximations to the thermal density matrix in order to compute the convolution efficiently. The simplest of the approximations is to assume that the kinetic-energy operator ($\mathcal{T}$) and the potential-energy operator ($\mathcal{V}$) in the Hamiltonian commute with each other. As $\tau \to 0$ or equivalently as $PT \to \infty$, the "primitive approximation" is given by:

$$e^{-\tau(\mathcal{T}+\mathcal{V})} \approx e^{-\tau \mathcal{T}} e^{-\tau \mathcal{V}} \tag{4}$$

The Trotter formula proves that this approximation does converge to the right result in the $P \to \infty$ limit and is given by:

$$e^{-\beta(\mathcal{T}+\mathcal{V})} = \lim_{P \to \infty} \left[e^{-\tau \mathcal{T}} e^{-\tau \mathcal{V}} \right]^P \tag{5}$$

It is worth noting that within the PI implementation, we are mainly interested in evaluating the trace of the density matrix, as it is directly related to the partition function. Also when using the primitive approximation, we neglect terms that are of the order τ^2. To improve the precision of results in MC simulations and to achieve faster convergence as P increases, higher order corrections (or propagators of the density matrix) have been developed.

The Takahashi-Imada (TI) propagator [4] with error of the order τ^4 uses:

$$\begin{aligned} Tr\left[e^{-\beta(\mathcal{T}+\mathcal{V})} \right] &= Tr\left[e^{-\frac{\beta}{P}\mathcal{T}} e^{-\frac{\beta}{P}\mathcal{V}'} \right]^P + O\left(\beta^5 P^{-4}\right), \\ \mathcal{V}' &= \mathcal{V} + \frac{1}{24} \left(\frac{\beta}{P} \right)^2 [\mathcal{V}, [\mathcal{T}, \mathcal{V}]]. \end{aligned} \tag{6}$$

Given a system with Hamiltonian $\mathcal{H}$ as:

$$\begin{aligned} \mathcal{H} &= \mathcal{T} + \mathcal{V}, \\ \mathcal{T} &= -\frac{\hbar^2}{2m}\sum_{i=1}^{N}\frac{\partial^2}{\partial \boldsymbol{r}_i^2}, \\ \mathcal{V} &= V(\boldsymbol{r}_1, \ldots, \boldsymbol{r}_N), \end{aligned} \tag{7}$$

it can be easily shown that from Eqs. (6) and (7), we get the following:

$$\mathcal{V}' = V(\boldsymbol{r}_1, \ldots, \boldsymbol{r}_N) + \frac{\hbar^2}{24m}\left(\frac{\beta}{P}\right)^2 \sum_{i=1}^{N} \left|\nabla_i V(\boldsymbol{r}_1, \ldots, \boldsymbol{r}_N)\right|^2, \tag{8}$$

where $\hbar$ is the reduced Planck's constant and ∇_i denotes the gradient with respect to coordinates of the ith atom. Equations (6) and (8) constitute the working equations of the TI propagator. Schenter [5] computed fully quantum virial coefficients using three different interaction potentials for water and found that using the semi-classical TI approximation (Eq. (8) with $P = 1$) gave the best agreement to fully quantum statistical mechanical calculations, especially at low temperatures where conventional expressions (based on the primitive approximation) including first order quantum corrections failed.

Janke and Sauer [6] showed that by adopting a slightly modified version of the Trotter formula (Eq. 5), they could systematically decrease the variance of the propagator. By decomposing the Hamiltonian to include more and more components of the kinetic- and potential-energy operators, they observed that the variance of the propagator improved. Suzuki [7] suggested new schemes for the exponential product formulae along with a basic theorem for a generalized decomposition that results in the propagator having error of the order $O(1/P^4)$. Yamamoto [8] showed that using a finite-difference based approach (instead of computing derivatives involved with the use of TI and Suzuki propagators) helped improve the variance further.

In this paper, we compute fully quantum virial coefficients of helium-4 using the TI propagator (Eqs. 6–8); we also consider the use of an ad hoc semi-classical potential (details of which will be explained in Sect. 4). Calculation of very precise physical properties of helium is of interest in the field of metrology to develop accurate calibration and pressure standards, to accurately compute the Boltzmann constant, and to improve acoustic gas thermometry [9–14]. Semi-classical virial coefficients up to fifth order have been computed for helium-4 by Shaul et al. [15], and showed that first-principles properties could be evaluated with precision and accuracy that exceeds experiment. Garberoglio and Harvey [9, 16, 17] reported fully quantum second and third virial coefficients for helium-3 and helium-4 including exchange effects where needed, for temperatures as low as 2.6 K. Shaul et al. [18] reported fully quantum virial coefficients of helium-4 (but without exchange) up to fourth order for temperatures of T = 2.6–1000 K.

The present application is primarily interested in demonstrating a variation of the PIMC methodology, rather than establishing new or more precise values of virial coefficients of helium. In Sect. 2 we will introduce the basics of computing quantum virial coefficients using PIMC. Sect. 3 explains how the thermal density matrix is used in PIMC to compute quantum virial coefficients. Sect. 4 contains all the simulation details including the ab initio Potential Energy Surface (PES) used, the range of temperatures investigated and other relevant computational parameters. Sect. 5 discusses the results and its comparison with values from literature, and also examines the performance of the various approaches used. We provide concluding remarks and ideas for future work in Sect. 6.

2 Quantum Virial Coefficients

Virial coefficients are important thermodynamic quantities of a system for two main reasons:

- They lead to other physical properties such as the pressure, critical temperature etc.
- They can be evaluated computationally given an interaction potential, and also by experiments. Thus the accuracy of the interaction potential can be judged based on the accuracy of the virial coefficients relative to experimental results.

The virial coefficients are generally denoted as B_N and the first two virial coefficients are given by [19]:

$$\begin{aligned} B_2(T) &= -\frac{1}{2!\underline{V}}\left[Z_2^* - Z_1^{*2}\right], \\ B_3(T) &= -\frac{1}{3!\underline{V}^2}\left[\underline{V}(Z_3^* - 3Z_2^*Z_1^* + 2Z_1^{*3}) - 3(Z_2^* - Z_1^{*2})^2\right], \end{aligned} \tag{9}$$

where $Z_N^* \equiv \left[N!\left(\frac{V}{Q_1}\right)^N Q_N\right]$ is the N-body configurational integral, Q_N is the N-body canonical partition function, and $\underline{V}$ is the volume.

The N-body configurational integral, which depends on the N-body interaction potential, becomes exponentially more difficult to compute with increasing N. For extremely simple interaction potentials like hard spheres, up to fourth-order virial coefficients may be calculated analytically [20]. Higher order virial coefficients using more complicated interaction potentials need to be evaluated numerically through quadrature or by using MC simulations. Upon further simplification and assuming pairwise additivity of the potential, we can rewrite Eq. (9) using Mayer f-functions as [20, 21]:

$$B_2(T) = -\frac{1}{2}\int \mathrm{d}1\, f(0,1),$$
$$B_3(T) = -\frac{1}{3}\iint \mathrm{d}1\ \mathrm{d}2\, f(0,1)\, f(0,2)\, f(1,2), \tag{10}$$

where $f(0,1) = (\exp[-\beta U_2(\boldsymbol{r})] - 1)$ and indices '1' and '2' denote the position and orientational degrees of freedom of molecules 1 and 2, respectively, with respect to molecule '0' at the origin.

Empirical potentials, which are usually functions that are fit to experimental data, tend to predict the net effect of a variety of phenomena over a range of conditions, and are consequently less accurate than ab initio PES for describing N-body interactions. The virial coefficients that are calculated from an input interaction potential (empirical or ab initio PES) without modification are known as classical virial coefficients because they do not include nuclear quantum effects explicitly. Virial coefficients computed using an effective potential such as the Quadratic Feynman-Hibbs (QFH) [1] that includes a quantum correction are known as semi-classical virial coefficients.

Nuclear quantum effects are almost always ignored in the development of an ab initio PES because of the Born-Oppenheimer approximation, which greatly simplifies the electronic Schrödinger equation by separating or decoupling the coordinates of the electrons from those of the nuclei. However, quantum mechanics prescribes that the wave functions of the atoms/molecules become more diffuse at low temperatures, or in other words, they become "fuzzy." This behavior has an effect on the virial coefficient. Therefore, when using ab initio PESs for the calculation of physical properties, especially at low temperatures, one needs to account for the nuclear quantum effects explicitly. The discretized PI formalism of Feynman provides a route to approximate the inherent fuzziness of an atom/molecule at low temperatures as a closed ring of 'beads' that represent the atom/molecule at P different imaginary-time instances. The formalism maps the quantum mechanical partition function onto the classical partition function of a closed ring polymer with P beads where adjacent beads are connected by harmonic springs whose stiffness depends on the temperature, atomic mass and P. The larger the discretization parameter P, the better the characterization of the fuzziness.

PIMC involves simulating different configurations of the closed ring polymer and accepting/rejecting it based on some MC criteria. The property of interest (usually the interaction potential) is then averaged across the simulation with each configuration having an appropriate weight. The interaction potential between two molecules is defined to be the average of the inter-molecular potential energy over corresponding beads of the two rings. Virial coefficients that are calculated from an input interaction potential including nuclear quantum effects using PIMC method are therefore known as (fully) quantum virial coefficients.

3 Thermal Density Matrix and PIMC

In this section, we will show how the thermal density matrix is used in PIMC to compute quantum virial coefficients. Consider the Hamiltonian of a monatomic molecule like helium with mass m (Eq. 7). Using the primitive approximation (Eq. 4), Trotter formula (Eq. 5), and following the procedure outlined in Ref. [9], we can obtain the kinetic-energy operator matrix elements as:

$$\left\langle \boldsymbol{r}_i \middle| \exp\left(-\frac{\beta \hat{p}^2}{2mP}\right) \middle| \boldsymbol{r}_j \right\rangle = \frac{P^{3/2}}{\Lambda^3} \exp\left(-\frac{K(\boldsymbol{r}_i - \boldsymbol{r}_j)^2}{2}\right), \tag{11}$$

where $K = \frac{2\pi P}{\Lambda^2}$, $\Lambda = \frac{h}{\sqrt{2\pi m k_B T}}$.

The potential-energy operator matrix elements can similarly be written as [3]:

$$\left\langle \boldsymbol{r}_i \middle| \exp\left(-\frac{\beta V(\boldsymbol{r})}{P}\right) \middle| \boldsymbol{r}_j \right\rangle = \exp\left(-\frac{\beta V(\boldsymbol{r}_i)}{P}\right) \delta(\boldsymbol{r}_i - \boldsymbol{r}_j). \tag{12}$$

It can be easily shown [9] then that the expression for the fully quantum second virial coefficient can be written as:

$$B_2(T) = -2\pi \int \mathrm{d}r\, r^2 (e^{-\beta V_{2,\mathrm{eff}}(r)} - 1), \tag{13}$$

where

$$e^{-\beta V_{2,\mathrm{eff}}(r)} = \int \prod_{i=1}^{P-1} \mathrm{d}^3 \Delta \boldsymbol{r}_i \, e^{-\beta \overline{U}_2(r)} \, F_{\mathrm{ring}}(m; \Delta \boldsymbol{r}_1, \ldots, \Delta \boldsymbol{r}_{P-1}), \tag{14}$$

$$\begin{aligned} \overline{U}_2(r) &= \frac{1}{P} \sum_{i=1}^{P} U_2(\boldsymbol{r}_{1,i}, \boldsymbol{r}_{2,i}), \\ |r|^2 &= |\boldsymbol{r}_1^{cm} - \boldsymbol{r}_2^{cm}|^2, \, \boldsymbol{r}_i^{cm} \equiv \frac{1}{P} \sum_{j=1}^{P} \boldsymbol{r}_{i,j} \end{aligned} \tag{15}$$

$$\begin{aligned} F_{\mathrm{ring}}(m; \Delta \boldsymbol{r}_1, \ldots, \Delta \boldsymbol{r}_{P-1}) &= \Lambda^3 \left(\frac{P^{3/2}}{\Lambda^3}\right)^P \exp\left[-\frac{K}{2} \sum_{i=1}^{P} \Delta \boldsymbol{r}_i^2\right], \\ \Delta \boldsymbol{r}_i &= \boldsymbol{r}_{i+1} - \boldsymbol{r}_i \, (i = 1, \ldots, P-1). \end{aligned} \tag{16}$$

Here $F_{\mathrm{ring}}(m; \Delta \boldsymbol{r}_1, \ldots, \Delta \boldsymbol{r}_{P-1})$ represents the weight of a ring polymer configuration, $U_2(\boldsymbol{r}_{1,i}, \boldsymbol{r}_{2,i})$ is the inter-molecular potential energy between the ith beads of rings 1 and 2, $V_{2,\mathrm{eff}}(r)$ is an effective inter-molecular potential defined by Eq. (14) and r is the inter-molecular separation.

The kinetic-energy operator in the Hamiltonian gives rise to the weight of the ring configuration, which depends on the harmonic energy of the system with P beads. The potential-energy operator (and hence, the ab initio PES) leads to the effective potential $V_{2,\mathrm{eff}}(r)$ in the expression for the quantum virial coefficient. Recall that we used the primitive approximation where the potential-energy operator was a simple function of the PES. If instead, we were to include higher order terms in the primitive approximation using the TI propagator, we would expect it to affect only $\overline{U}_2(r)$. This would in turn lead to a change in the effective potential $V_{2,\mathrm{eff}}(r)$. From Eqs. (7) and (8), Eq. (15) can be rewritten as follows:

$$\overline{U}_2(r) = \frac{1}{P}\sum_{i=1}^{P}\left[U_2(\boldsymbol{r}_{1,i},\boldsymbol{r}_{2,i}) + \frac{\hbar^2}{24m}\left(\frac{\beta}{P}\right)^2 |\nabla U_2(\boldsymbol{r}_{1,i},\boldsymbol{r}_{2,i})|^2\right]. \tag{17}$$

We can see that the argument within the sum on the right-hand side of the expression for $\overline{U}_2(r)$ goes from being a quantity completely independent of P and $\hbar$ as in Eq. (15) to a quantity that is dependent on both P and $\hbar$ as in Eq. (17). The inter-molecular potential experienced by the beads of the ring changes from being classical to semi-classical (dependent on P and $\hbar$). Therefore, the phrase 'PIMC with **semi-classical beads**' along with Fig. 1 is an apt description of such a PIMC

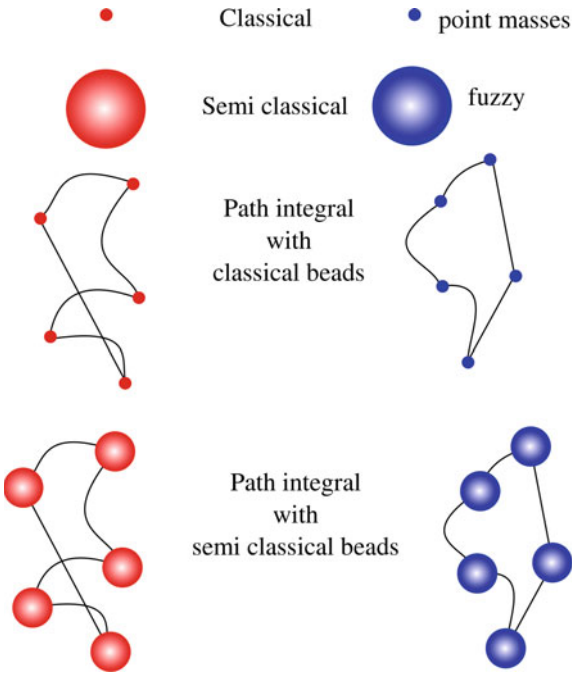

Fig. 1 Different levels of "quantumness" of a B_2 calculation going from classical virial coefficients that are calculated assuming point masses to fully quantum virial coefficients with semi-classical beads. The different sphere sizes here are for illustrative purposes only and no quantitative inference should be made

simulation. For a fixed P, we would expect to capture more quantum effects with the use of semi-classical beads than classical beads, that is, by using the primitive approximation with higher order terms than just the primitive approximation by itself.

4 Computational Details

In Sect. 3 we noted that using different propagators brought about changes only in the effective potential used. While a given propagator will correspond to some effective potential, the converse might not necessarily be true—selection of an ad hoc effective potential might not map back to an appropriate propagator. Still, it may be interesting to examine other choices of semi-classical potential for use in a PIMC framework, without deriving it from a propagator. Once the accuracy of such an ad hoc potential is established empirically, we can then compare its efficiency against the TI propagator. We have in mind in particular the QFH effective potential [1, 5], modified slightly for this purpose. We denote this as QFH* and it is given as:

$$U_2^{\mathrm{QFH}^*}(\boldsymbol{r}_{1,i},\boldsymbol{r}_{2,i}) = U_2(\boldsymbol{r}_{1,i},\boldsymbol{r}_{2,i}) + \frac{\hbar^2\beta}{24mP^2}\left[\frac{\partial^2 U_2(\boldsymbol{r}_{1,i},\boldsymbol{r}_{2,i})}{\partial r_{12,i}^2} + \frac{2}{r_{12,i}}\frac{\partial U_2(\boldsymbol{r}_{1,i},\boldsymbol{r}_{2,i})}{\partial r_{12,i}}\right],$$
$$|r_{12,i}|^2 = |\boldsymbol{r}_{1,i} - \boldsymbol{r}_{2,i}|^2 \tag{18}$$

where m is the mass of the atom. We use the $1/P^2$ prefactor for the second term as it closely resembles the TI propagator and also gives the best results of those we examined. The standard QFH semi-classical potential is obtained for $P = 1$.

The ab initio helium pair potential that we used is due to Przybytek et al. [22] (denoted as u) and a simplified, approximate version of the same (denoted as u^{simple}) was obtained from supplementary material of Shaul et al. [18]. We investigated a total of 8 temperatures ranging from T = 2.5–500 K. Mayer Sampling Monte Carlo (MSMC) [23, 24], which uses importance sampling to compute virial coefficients efficiently for any given interaction potential, was employed in our calculations.

Since this work is aimed at extending the work of Shaul et al. [18], we shall be comparing the performance of the TI propagator and the QFH* effective potential against their results. In order to make a fair and consistent comparison, we employ the same decomposition algorithms as Shaul et al. [18]. These schemes were developed to improve the efficiency of the virial coefficient calculation, doing so by computing the full quantum virial coefficients through a series of stages of increasing accuracy in the quantum treatment and adherence to the target PES. We have the same three choices for the preliminary approximation: (1) semi-classical, $[\Gamma^{\mathrm{SCL}}(u)]$, (2) the u^{simple} approximation to the semi-classical treatment, $[\Gamma^{\mathrm{SCL}}(u^{\mathrm{simple}})]$ and (3) the u^{simple} approximation to u for a finite P, $[\Gamma(P, u^{\mathrm{simple}})]$.

Here Γ represents the configurational integral of the associated potential, the square brackets indicate an independent simulation, and the superscript SCL denotes a QFH semi-classical approximation (Eq. 18) to u or u^{simple}. Since we are interested only in B_2, the Percus-Yevick compressibility route approximation [21, 25, 26] to the semi-classical approximation is ignored.

Any computational details regarding the inter-molecular potentials, decomposition strategies and MSMC parameters that are not included here may be found in Sect. B of Shaul et al. [18] and the supplementary material therein.

5 Results

For ease of reference and use, we note and define the following:

- All the simulations involved the same set of inter-molecular potentials, u or u^{simple} or their semi-classical approximations.
- We denote quantum virial coefficient results from Shaul et al. [18] as B_2^{cl}, those using the QFH* effective potential as $B_2^{\text{sc,QFH}^*}$, and those using the TI propagator as $B_2^{\text{sc,TI}}$; the first part of the superscript denotes which type of beads (classical (cl) or semi-classical (sc)) were used in the PIMC calculations. Note this is not to be confused with the preliminary approximations $[\Gamma^{\text{SCL}}(u)]$ or $[\Gamma^{\text{SCL}}(u^{\text{simple}})]$ which denote the semi-classical calculations using the QFH approximations to u and u^{simple} respectively.
- In the same spirit, we refer to the algorithm for computing B_2^{cl} as the Classical Beads approach denoted as CB; $B_2^{\text{sc,QFH}^*}$ as the Semi-Classical Beads QFH* approach denoted as SCB-QFH*; $B_2^{\text{sc,TI}}$ as the Semi-Classical Beads TI approach denoted as SCB-TI.
- It is possible to use a semi-classical TI approximation ($P = 1$ in Eq. (8)) instead of the QFH (Eq. 18) approximation while using the TI propagator. However, after performing several calculations, we observed that using semi-classical TI approximations as preliminary approximations always led to inefficient decompositions, which resulted in larger uncertainties in $B_2^{\text{sc,TI}}$ than B_2^{cl} or $B_2^{\text{sc,QFH}^*}$. This is because the uncertainty of the quantity $y = [\Gamma(P, u^{\text{simple}}) - \Gamma^{\text{SCL}}(u^{\text{simple}})]$, was significantly higher when using the semi-classical TI approximation than its QFH counterpart. Hence, we decided to use the semi-classical QFH approximation while using both the TI propagator as well as QFH* effective potential.

We know that all propagators yield results that converge to the correct value in the $P \to \infty$ limit, irrespective of the choice of the potential. So, as a first step, we verified that the $B_2^{\text{sc,QFH}^*}$ did agree within statistical uncertainties with B_2^{cl}. In the next step, we break down our $B_2^{\text{sc,QFH}^*}$ and $B_2^{\text{sc,TI}}$ simulations into smaller, more

precise ones using the decomposition algorithm. We observed a similar trend for $B_2^{\mathrm{sc,QFH}^*}$ and $B_2^{\mathrm{sc,TI}}$ decompositions as was observed [18] for B_2^{cl}, i.e. for $T > 63.15\,\mathrm{K}$ $[\Gamma^{\mathrm{SCL}}(u)]$ is always chosen as the preliminary approximation, for $4K \leq T \leq 63.15\,\mathrm{K}$ $[\Gamma^{\mathrm{SCL}}(u^{\mathrm{simple}})]$ is chosen as the preliminary approximation and for $T < 4\,\mathrm{K}$ $[\Gamma(P, u^{\mathrm{simple}})]$ is chosen as the preliminary approximation.

To assess the performance of SCB-QFH* and SCB-TI approaches against the CB approach in terms of achieving faster convergence as P increases, in Fig. 2, we plot the magnitude of $y = [\Gamma(P, u) - \Gamma(P/2, u)]$ as a function of P. For convergence to be achieved, as P increases $|y|$ decreases and as $P \to \infty, |y| \to 0$; the smaller the value of $|y|$, the faster the convergence. In Fig. 2 we see that the SCB-TI values are consistently lower than values of the other two approaches for all temperatures except T = 10.0 and 50.0 K for P = 4 beads, where the SCB-QFH* has lower $|y|$ values than SCB-TI. This condition is not particularly relevant, because at lower temperatures we almost always use a value of $P > 4$ and the convergence is more dependent on $|y|$ values for higher P (128 say), where SCB-TI has much lower $|y|$ values. From Fig. 2 we also notice that as temperature increases, $|y|$ decreases for each case. This is to be expected, because as we increase temperature the system approaches classical behavior, requiring fewer and fewer beads to converge.

To assess the performance of SCB-QFH* and SCB-TI approaches against the CB approach in terms of achieving better precision, we plot the ratios of uncertainty of the quantity $y = [\Gamma(P, u) - \Gamma(P/2, u)]$, i.e. we plot σ_y (SCB-QFH*)/σ_y(CB) and σ_y (SCB-TI)/σ_y(CB) in Fig. 3. In order to make a fair comparison, we use the uncertainties due to the same number of MC steps (1×10^6) for each case. In Fig. 3

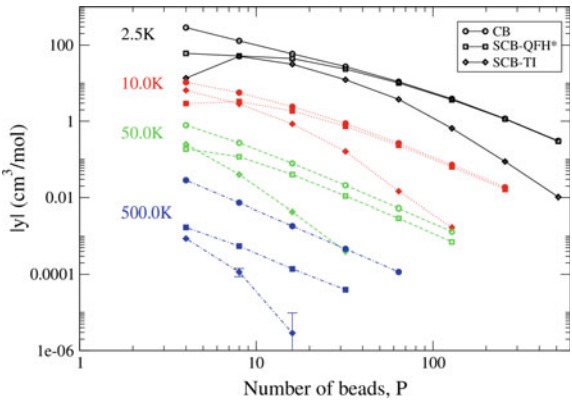

Fig. 2 Convergence factor, $y = [\Gamma(P, u) - \Gamma(P/2, u)]$ as a function of number of beads P. Symbols alternate filled or open with each temperature and indicate: classical-beads (CB) approach (*circles*); SCB-QFH* (*squares*); SCB-TI (*diamonds*). Temperatures are $T =$ 2.5 K (*black open symbols* connected by *solid lines*); $T = 10.0$ K (*red filled symbols* connected by *dotted lines*); $T = 50.0$ K (*green open symbols* connected by *dashed lines*); $T = 500.0$ K (*blue filled symbols* connected by *dash-dot lines*). Confidence limits (68 %) are smaller than the symbol sizes except where shown

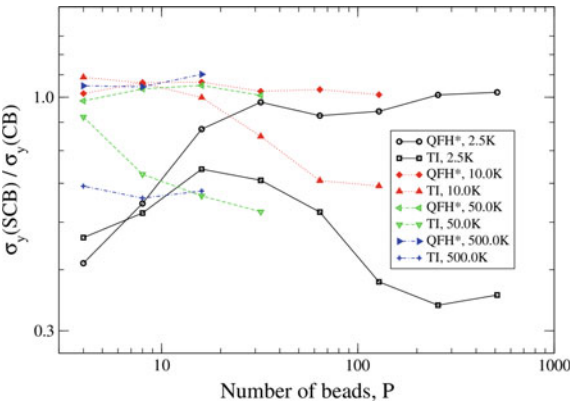

Fig. 3 Uncertainty ratio of the convergence factor $\sigma_y(\mathrm{SCB})/\sigma_y(\mathrm{CB})$, where $y = [\Gamma(P,u) - \Gamma(P/2,u)]$, as a function of number of beads P

we observe that SCB-TI has a consistently lower uncertainty ratio than SCB-QFH* for all P except for $P = 4$, where the $T = 2.5$ and 5.0 K results for SCB-QFH* have slightly lower values. At these low temperatures, since $P > 4$ almost always, we do not worry too much about SCB-QFH* having lower uncertainty ratios because it does not affect the uncertainty of the overall result that much, and also because the values are only slightly lower. The ratio for SCB-QFH* is almost always greater than 1, suggesting that it is not expected to give better precision when compared to CB for most cases. For the cases where the SCB-QFH* ratio is less than 1, i.e. $T = 2.5$ K and $P \leq 128$, we expect it to give better precision. The ratio for SCB-TI is almost always less than 1, suggesting that it is expected to give better precision when compared to CB for most cases. For the cases where the SCB-TI ratio is greater than 1, i.e. $T = 10.0$ K and $P \leq 8$, the magnitude is only marginally greater; as explained earlier, usually $P > 8$ is needed for accurate results when $T = 10.0$ K.

To assess the performance of SCB-QFH* and SCB-TI approaches against the CB approach in terms of the uncertainty achieved for a given period of time, in Fig. 4 we plot the ratios of the best-case uncertainties of the quantum second virial

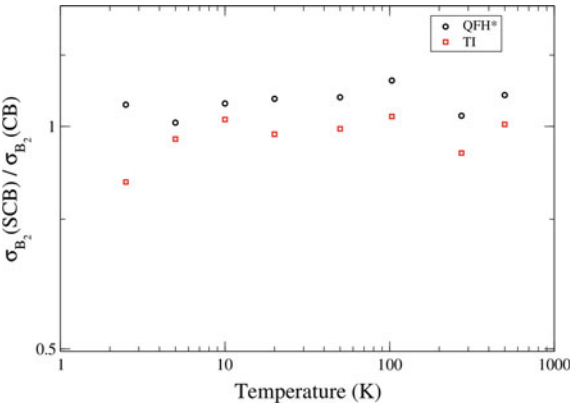

Fig. 4 Uncertainty ratio $\sigma_{B_2}(\mathrm{SCB})/\sigma_{B_2}(\mathrm{CB})$ as a function of temperature, for optimal decomposition with a fixed total computation time of 1 CPU-hour

coefficient values resulting from an overall simulation time of 1 h, i.e. we plot $\sigma_{B_2}(\text{SCB - QFH}^*)/\sigma_{B_2}(\text{CB})$ and $\sigma_{B_2}(\text{SCB} - \text{TI})/\sigma_{B_2}(\text{CB})$ calculated after optimally decomposing the simulation effort for a cumulative time of 1 h. We again observe that in Fig. 4, the SCB-TI approach has a lower uncertainty ratio than SCB-QFH* for all temperatures considered. Also, the ratio of SCB-TI is slightly less than 1 for most cases while that of SCB-QFH* is always greater than 1. This suggests that decomposition for the SCB-QFH* approach is expected to yield larger uncertainties for the quantum virial coefficient, compared to that of CB and SCB-TI approaches. The decomposition for the SCB-TI approach seems to be performing better than the SCB-QFH* approach, especially at lower temperatures, which is desirable because we normally tend to use large P at these temperatures. Even in the cases where the SCB-TI ratio is greater than 1, it is only marginally greater and therefore it may be considered acceptable.

6 Conclusion

We have implemented the PIMC method with two approaches based on semi-classical beads (SCB-QFH*, SCB-TI) and MSMC to compute more precise quantum virial coefficients for helium-4. The SCB results agree well with CB results as they are within statistical uncertainties of each other. The decomposition algorithm of Shaul et al. [18] was implemented to achieve better efficiency of quantum virial coefficient calculations. We observed similar trends in decompositions of simulations in our SCB based approaches as was the case for the CB approach. For lower temperatures, the approximation u^{simple} to u for finite P is chosen as the preliminary approximation. As the temperature increases, the preliminary approximation preferred is the semi-classical approximation to u^{simple}, and for high temperatures the semi-classical approximation to u is preferred. Having chosen the preliminary approximation, the decomposition algorithm spends the most time in the first step and the amount of time spent per step gradually decreases for subsequent steps. This is because the subsequent steps involve more computationally expensive calculations (either by shifting to u from its semi-classical approximation, or by doubling P from the previous step, or by shifting to the full potential u from u^{simple}) and by design, these steps also yield better and better precision. The decomposition algorithm was designed to allocate computational effort proportional to the difficulty of the computation, which is defined as $((\text{cpu-time})^{1/2} \times \text{uncertainty})$. The SCB-QFH* and SCB-TI approaches have comparable and better uncertainties respectively, for the steps that involve computing $[\Gamma(P,u) - \Gamma(P/2,u)]$ or $[\Gamma(P,u^{\text{simple}}) - \Gamma(P/2,u^{\text{simple}})]$. Since these steps involve significant computational costs and relatively low uncertainties, the amount of effort dedicated for them is lower, attenuating the effect of any efficiency brought to their calculation. As a result, the improvement of the precision of the resulting virial coefficient is only marginal. We note that if the decomposition algorithm is

not being used, either because it is non-trivial to apply, or because virial coefficients are not being computed, the SCB-TI approach performs much better than both SCB-QFH* and CB approaches, which is what we would expect anyway from the use of a higher order propagator.

In summary, we found the following order for the rate of convergence with respect to number of beads P: SCB-TI > SCB-QFH* > CB. We expect a similar trend for the rate of convergence with respect to P for higher order coefficients as well, because of the use of the higher order TI propagator. The order for precision was found to be: SCB-TI > SCB-QFH*. Compared to CB, QFH* is always worse but only marginally so; TI is almost always better and only marginally worse for a few temperatures. We expected a trend similar to the rate of convergence with P for the precision as well, even for B_2 calculations. Since this was not what we observed, partially due to the decomposition algorithm, an understanding of the order of precision for higher order coefficients for the SCB based approaches compared to CB approach would require further investigation. However, we do expect the order between SCB based approaches to remain the same, i.e., SCB-TI > SCB-QFH*.

Directions for future work include investigating more temperatures, comparing the performance of different higher-order propagators of the thermal density matrix in terms of precision and rate of convergence, and using alternative ab initio potentials as they become available. Extension of PIMC with semi-classical beads to multi-atomic molecules is straightforward, and we expect such an approach to perform better than conventional PIMC with classical beads, in terms of convergence rate and precision.

Acknowledgments This work is supported by the U.S. National Science Foundation (CHE-1027963).

References

1. Feynman, R.P., Hibbs, A.R.: Quantum Mechanics and Path Integrals, 1st edn. McGraw-Hill Companies, Inc., New York (1965). Emended by Daniel F. Styer
2. Ceperley, D.: Path integrals in the theory of condensed helium. Rev. Mod. Phys. **67**, 279 (1995)
3. Cui, T., Cheng, E., Alder, B., Whaley, K.: Rotational ordering in solid deuterium and hydrogen: a path integral Monte Carlo study. Phys. Rev. B **55**, 12253 (1997)
4. Takahashi, M., Imada, M.: Monte Carlo calculation of quantum systems. II. higher order correction. J. Phys. Soc. Jpn. **53**, 3765–3769 (1984)
5. Schenter, G.K.: The development of effective classical potentials and the quantum statistical mechanical second virial coefficient of water. J. Chem. Phys. **117**, 6573 (2002)
6. Janke, W., Sauer, T.: Properties of higher-order Trotter formulas. Phys. Lett. A **165**, 199–205 (1992)
7. Suzuki, M.: Hybrid exponential product formulas for unbounded operators with possible applications to Monte Carlo simulations. Phys. Lett. A **201**, 425–428 (1995)
8. Yamamoto, T.M.: Path-integral virial estimator based on the scaling of fluctuation coordinates: application to quantum clusters with fourth-order propagators. J. Chem. Phys. **123**, 104101 (2005)

9. Garberoglio, G., Harvey, A.H.: First-principles calculation of the third virial coefficient of helium. J. Res. Natl. Inst. Stand. Technol. **114**, 249 (2009)
10. Fellmuth, B., Gaiser, C., Fischer, J.: Determination of the Boltzmann constant—status and prospects. Meas. Sci. Technol. **17**, R145–R159 (2006)
11. Schmidt, J.W., Gavioso, R.M., May, E.F., Moldover, M.R.: Polarizability of helium and gas metrology. Phys. Rev. Lett. **98**, 254504 (2007)
12. Pitre, L., Moldover, M.R., Tew, W.L.: Acoustic thermometry: new results from 273 K to 77 K and progress towards 4K. Metrologia **43**, 142–162 (2006)
13. Moldover, M.R., McLinden, M.O.: Using *ab initio* data to accurately determine the fourth density virial coefficient of helium. J. Chem. Thermodyn. **42**, 1193–1203 (2010)
14. Aziz, R.A., Janzen, A.R., Moldover, M.R.: *Ab initio* calculations for helium: a standard for transport property measurements. Phys. Rev. Lett. **74**, 1586–1589 (1995)
15. Shaul, K.R.S., Schultz, A.J., Kofke, D.A., Moldover, M.R.: Semiclassical fifth virial coefficients for improved *ab initio* helium-4 standards. Chem. Phys. Lett. **531**, 11–17 (2012)
16. Garberoglio, G., Harvey, A.H.: Path-integral calculation of the third virial coefficient of quantum gases at low temperatures. J. Chem. Phys. **134**, 134106 (2011)
17. Garberoglio, G., Moldover, M.R., Harvey, A.H.: Improved first-principles calculation of the third virial coefficient of helium. J. Res. Natl. Inst. Stand. Technol. **116**, 729–742 (2011)
18. Shaul, K.R., Schultz, A.J., Kofke, D.A.: Path-integral Mayer-sampling calculations of the quantum Boltzmann contribution to virial coefficients of helium-4. J. Chem. Phys. **137**, 184101 (2012)
19. Tester, J.W., Modell, M.: Thermodynamics and Its applications, 3rd edn. Prentice Hall Inc, New Jersey (1997)
20. Masters, A.J.: Virial expansions. J. Phys.: Condens. Matter **20**, 283102 (2008)
21. Hansen, J.P., McDonald, I.R.: Theory of Simple Liquids, 3rd edn. Academic Press (2006)
22. Przybytek, M., Cencek, W., Komasa, J., Łach, G., Jeziorski, B., Szalewicz, K.: Relativistic and quantum electrodynamics effects in the helium pair potential. Phys. Rev. Lett. **104**, 183003 (2010)
23. Singh, J.K., Kofke, D.A.: Mayer sampling: calculation of cluster integrals using free-energy perturbation methods. Phys. Rev. Lett. **92**, 220601 (2004)
24. Schultz, A.J., Kofke, D.A.: Sixth, seventh and eighth virial coefficients of the Lennard-Jones model. Mol. Phys. **107**, 2309 (2009)
25. Percus, J.K., Yevick, G.J.: Analysis of classical statistical mechanics by means of collective coordinates. Phys. Rev. **110**, 1–13 (1958)
26. Shaul, K.R.S., Schultz, A.J., Perera, A., Kofke, D.A.: Integral-equation theories and Mayer-sampling Monte Carlo: a tandem approach for computing virial coefficients of simple fluids. Mol. Phys. **109**, 2395–2406 (2011)